# Variability of eddy-driven jets and their interaction with the subtropical Hadley-driven jet

Elizabeth A. Barnes * and Dennis L. Hartmann

*Department of Atmospheric Sciences, University of Washington, Seattle, Washington*

* *Corresponding author address:* Elizabeth A. Barnes, Department of Atmospheric Sciences, University of Washington, Box 351640, Seattle, WA 98195.

E-mail: eabarnes@atmos.washington.edu

ABSTRACT

The eddy-driven jet is located in the midlatitudes, bounded on one side by the pole and often bounded on the opposite side by a strong Hadley-driven jet. This work explores how the eddy-driven jet and its variability persist within these limits. It is demonstrated in a barotropic model that as the jet is located at higher latitudes, the leading mode of variability of the jet changes from a meridional shift to a pulse, and the eddy-length scale increases, consistent with the Rhines-scale prediction. Looking equatorward, a similar change in eddy-driven jet variability is observed when a constant subtropical jet is moved toward the eddy-driven jet in midlatitudes. In both the poleward and equatorward limits, the change in variability from a shift to a pulse is due to the modulation of eddy propagation and momentum flux. Near the pole, the small value of beta and subsequent lack of wavebreaking near the pole accounts for the change in variability, whereas on the equatorward side of the jet, the strong subtropical winds affect eddy propagation and actually force the midlatitude jet poleward. This work suggests that the expansion of the Hadley cell may be enough to cause the eddy-driven jets to shift poleward with climate change, and that the leading mode of zonal-wind variability will transition from a shift to a pulse as the jet moves poleward.

# 1. Introduction

The eddy-driven jet and its variability exist within the region between the pole and the Hadley-driven subtropical jet. While the leading mode of variability of the eddy-driven jet is often associated with a meridional shifting of the zonal-mean zonal winds, Eichelberger and Hartmann (2007) showed in a simple general circulation model that in the presence of a strong subtropical jet, the leading mode describes a pulsing of the eddy-driven jet. In the other limit, recent studies have shown that the variability of the eddy-driven jet also changes from a shift to a pulse as the jet moves poleward, with the persistence of the variability also decreasing with latitude (Kidston and Gerber 2010; Barnes et al. 2010; Barnes and Hartmann 2010).

The goal of this work is to investigate one overarching question: "What are the equatorward and poleward constraints on eddy-driven jet variability?" More specifically, we will focus on the following questions:

- Why does the variability of the jet change from a shifting to a pulsing in the presence of a strong Hadley-driven jet?

- Why does the variability of the jet change from a shifting to a pulsing as the eddy-driven jet is moved poleward?

- How does the scale of the eddies change as the jet shifts poleward?

- How do changes in jet variability relate to changes in eddy-mean flow feedbacks and persistence?

To answer these questions, we employ a stochastically stirred barotropic model to mimic

a midlatitude storm track. A barotropic model is a good vehicle for understanding annular mode variability because these modes require meridional transport of momentum by eddies as a fundamental process for their existence. Meridional wave propagation and wave, mean-flow interaction theory are therefore central and well captured in a barotropic model. In this context, meridionally-confined stirring in a barotropic model is a reasonable analogue for a baroclinic storm track, since in both cases the generation of the eddies is maximum in the jet core, and it is the meridional fluxes into and out of the jet that are critical.

## 2. Methods

We follow Vallis et al. (2004); Barnes et al. (2010) and integrate the spectral non-divergent barotropic vorticity equation on the sphere,

$$\frac{\partial \zeta}{\partial t} + u\frac{\partial \zeta}{\partial x} + v\frac{\partial \zeta}{\partial y} + v\beta = \mathcal{S} - r\zeta - \kappa\nabla^4\zeta, \tag{1}$$

where r is the damping parameter set equal to 1/6 days$^{-1}$ and $\kappa$ is the diffusion coefficient for parameterizing the removal of enstrophy at small scales. The model is run at a resolution of T42 and atmospheric eddies are modeled as an Ornstein-Uhlenbeck stochastic process ($\mathcal{S}$) defined for each combination of total wavenumber $l$ and zonal wavenumber $m$:

$$\mathcal{S}_{lm} = (1 - e^{2dt/\tau})^{1/2} Q^i + e^{-dt/\tau}\mathcal{S}_{lm}^{i-1}, \tag{2}$$

where $\tau$ denotes the decorrelation time of the stirring and $Q^i$ is a real number chosen uniformally between $(-\mathcal{A}, \mathcal{A}) \times 10^{-11}$, where $\mathcal{A}$ is the stirring strength (see Vallis et al. (2004) for details). The model is stirred over a range of total wavenumbers, and the sensitivity of the results on the stirring range will be discussed in detail in Section 3. Finally, to mimic a

meridionally-confined "storm track", the gridded stirring field is windowed in the meridional direction with a Gaussian spatial mask centered at latitude $\theta_{stir}$ and having a half-width of 12$^o$for all integrations.

The model is integrated from pole-to-pole, but since the stirring is located in only one hemisphere, we restrict our analysis to that half of the globe. Each integration is spun-up for at least 500 days and then integrated an additional 12000 days for analysis. To aid the reader, we have compiled a list of variables used regularly in our discussion and have defined them in Table 1.

# 3. Eddy-length scale

Much of this work investigates the interaction between syntopic-scale eddies and the larger-scale mean flow. Eddy wave propagation and the resulting momentum fluxes are strongly dependent on the scale of the eddies themselves, and as such, we begin by determining the dependence of this scale on latitude. In addition, we demonstrate an optimal eddy-length scale for driving a strong, westerly jet.

*a. Change in eddy-length scale with latitude*

A common scaling for eddies is the halting scale of the geostrophic inverse cascade, often predicted by the Rhines scale $L_R$ (Rhines 1975). We can convert this to a scaling for the non-dimensional eddy wavenumber

$$l_R = aL_R^{-1} = a\left(\frac{\beta}{U_{rms}}\right)^{1/2}, \tag{3}$$

where $a$ is the radius of the earth and $U_{rms}$ is the root-mean-square zonal flow. (3) predicts that as $\beta$ decreases toward the pole, the characteristic eddy wavenumber will decrease (length scale will increase), assuming the zonal wind strength stays approximately constant.

To test the scaling predicted by (3), the model is stirred at multiple latitudes to test whether the latitude of the jet influences the scale of the Rossby waves. The wavenumbers over which the model is stirred can effect the resulting eddy-scale, and as such, we stir the model with *white noise*, constructed such that each wavenumber pair $(l, m)$ is stirred identically, where $l$ is the total wavenumber of a spherical harmonic expansion of vorticity. We stir over wavenumbers $1 \leq l \leq 42$ and $m \geq 1$ and window the stirring field with a Gaussian mask at varying $\theta_{stir}$ latitudes. The strength of the stirring is normalized by ensuring that the time-averaged energy injection rate of the stirring $(-\psi\mathcal{S})$ averaged over the hemisphere is constant across all integrations.

Work by Smith et al. (2002) shows that the strength of the linear drag can have large effects on the inverse cascade, and the results presented here set $r^{-1} = 6$ days. We have run additional experiments with $r^{-1} = 12$ days and $r^{-1} = 48$ days to confirm that the results are robust.

Fig. 1a shows the stirring total-wavenumber spectra for three characteristic integrations, and confirms that the stirring input is the same for each integration. The resulting vorticity spectra for the same integrations are displayed in Fig. 1b, where we have excluded the zonal-mean ($m = 0$) component to focus on the eddy contribution. Although the stirring spectrum is similar in all integrations, the peak of the vorticity spectrum shows a clear shift, such that when the jet is forced closer to the pole, the peak total wavenumber $\hat{l}$ shifts towards smaller values. To summarize this result, we define $\hat{l}$ from Fig. 1b by fitting a second-order

polynomial about the peak of the vorticity spectrum and finding the peak wavenumer. Fig. 1c shows $\hat{l}$ plotted against stirring latitude for 7 model integrations along with the theoretical prediction $l_R$ from (3).

Fig. 1c confirms that as the jet is forced at higher latitudes, the equilibrated Rossby wave length scale increases ($\hat{l}$ decreases). Perhaps more notably, the Rhines scaling predicts this scale reasonably well. Intuition would suggest that as $\beta$ decreases toward the pole, larger scale waves are needed to balance zonal advection with retrogression associated with $\beta$. Results presented here confirm that in the simplest case of the barotropic vorticity equation on the sphere, the Rossby wave scale increases as the jet moves to higher latitudes in a manner consistent with the Rhines scale prediction.

Work by Kidston et al. (2010) suggests that the eddy-length scale will increase by 3%-7% as the climate warms and the jets shift polewards. Interestingly, we find that the Rhines scaling presented here predicts that a typical jet moving from 46$^o$ to 48.5$^o$ will have an eddy scale change of about 5% due solely to the change in latitude of the jet. However, further work is required to determine whether this barotropic-scale argument is dominant in the real atmosphere.

*b. Importance of synoptic waves for driving a jet*

Fig. 1b demonstrates that even with white stirring, the equilibrium-eddy scale is skewed toward small wavenumbers. It is in fact these synoptic-scale Rossby waves that are responsible for the formation maintenance of a strong zonal jet. To demonstrate the sensitivity of the jet to eddy scale, the model is integrated for three different stirring configurations. In the

first integration, the model is stirred with *white noise*, defined previously as stirring $\mathcal{S}$ over total wavenumbers $1 \leq l \leq 42$. The second integration is termed *high-wavenumber* stirring and consists of scales smaller than those of synoptic eddies, specifically $10 \leq l \leq 42$. The third integration has *synoptic-scale* stirring, where the total wavenumber range is $4 \leq l \leq 10$. In all three integrations, the zonal wavenumber $m$ is confined to the same range as the total wavenumber $l$. As in previous experiments, a Gaussian mask with half-width 12$^{\text{o}}$ is applied to the stirring fields to mimic a localized storm track, and the stirring is centered at 45$^{\text{o}}$ N for all three integrations.

The stirring strength $\mathcal{A}$ for each run is defined such that the energy injection rate is constant across the integrations. Fig. 2a plots the prescribed stirring power versus total wavenumber for the three integrations. While we define the synoptic stirring experiment over wavenumbers 4 to 10, the resulting stirring spectrum exhibits power up to wavenumber 15. This apparent apparent inconsistency is due to the Gaussian window which slightly alters the final stirring spectrum on the high-wavenumber edge. We have confirmed that the latitude of the window does not affect the stirring spectum, but rather the spectrum is most sensitive to the width of the window, which remains constant throughout this work.

The resulting zonal-mean zonal winds for the three integrations are displayed in Fig. 2b. In the case of white noise stirring, a zonal-mean jet forms at the latitude of stirring with easterlies on both flanks, indicative of the presence of large-scale Rossby waves that are able to propagate and break to the north and south. The synoptic stirring integration also produces a zonal-mean jet, except the maximum winds are slightly poleward of the stirring. In the synoptic stirring integration, the easterlies on the poleward flank of the jet are much weaker compared to the white noise wind profile. The reason for this lies in

the fact that only very large-scale waves are able to propagate and decelerate near the pole as described in Section 4, and unlike the white noise stirring, the synoptic stirring omits wavenumbers 1-3. Thus, it is expected that easterlies will be weaker on the poleward flank of the synoptically-stirred jet.

The zonal-mean jet is forced by the propagation and breaking of Rossby waves, and it is the Rossby-wave scale that matter most for the formation and maintenance of the jet. In the integration where only high wavenumbers are stirred, the resulting jet is weak and equatorward of the region of stirring. These features are due to the inability of the small-scale waves to propagate and break near the pole. Thus, the equilibrium jet can only be sustained at a more equatorward latitude when the stirring-scale is smaller than that of synoptic waves.

We argue that the synoptic-scale Rossby waves are required to maintain a strong zonal jet, and the importance of synoptic-scales can be seen by the fact that the synoptic stirring produces a stronger jet than the white noise stirring, although the energy injection rate is identical for each. The difference lies in the forcing in the synoptic range, where the synoptic stirring has nearly 50% more power at these scales.

We have analyzed the vorticity spectra (not shown) and point out that $\hat{l}$ is similar in both the white noise and synoptic stirring integrations, as expected by an inverse energy cascade. However, in the case of the high-wavenumber stirring, the vorticity spectrum peaks around 19, and thus never reaches synoptic scales. This halting of the inverse cascade is likely due to the strong linear damping of $r^{-1} = 6$ days which Smith et al. (2002) argue can halt the cascade when friction dominates nonlinear advection.

Section Summary

- Synoptic-scale Rossby waves ($4 \leq l \leq 10$) are essential to the formation and maintenance of the eddy-driven jet.

- As the mean jet is located closer to the pole, the eddy-length scales must increase because of the need to balance zonal advection with retrogression associated with the small value of $\beta$. Model results confirm that this scale is reasonably predicted by the Rhines scale.

- The predicted change in eddy-length scale due only to a poleward shift of the jet agrees with scale changes seen in GCM global warming simulations.

# 4. Changes in the variability of the jet with latitude

Synoptic-scale eddies are critical in maintaining a strong zonal jet, and we have shown that the eddy-length scale increases with latitude. We now investigate the interactions between the eddies and the mean flow as the latitude of the jet is varied. Previous studies have shown that the latitude of the jet influences the persistence of meridionally shifts of the jet and that the leading mode of variability changes from a shift to a pulse as the mean jet is found closer to the pole (Barnes et al. 2010; Barnes and Hartmann 2010). In a baroptropic model, changes in the variability of the jet are solely due to changes in the eddy-mean flow interaction, and so in this section we investigate the effect of latitude on the pattern of jet variability and suggest a mechanism associated with changes in eddy-length scale and wave

propagation.

We integrate (1) on the sphere and stir the model over total wavenumbers $8 \leq l \leq 12$, but we require that $m \geq 4$ to ensure that we are not forcing at the scale of the zonal-mean flow itself. In Section 3 we showed that the formation of a jet is most dependent on these wavenumbers, however, white noise forcing was used for a selection of cases and it did not change the basic behavior. To determine the dependence of jet variability on latitude, $\theta_{stir}$ is varied in 5$^o$ increments between 35$^o$N and 65$^o$N giving rise to the formation of jets at varying latitudes. The stirring strength is held at a constant value for all integrations.

Fig. 3a displays the resulting zonal-mean, zonal-wind profiles for the most poleward and most equatorward $\theta_{stir}$. In both cases, the stirring produces a zonal-mean eddy-driven jet centered near the latitude of stirring. Defining the latitude of the jet, $\theta_{edj}$, as the mean of the time series of daily latitudes of maximum zonal-mean zonal winds ($Z_{lat}$), Fig. 4a shows that in all cases $\theta_{edj}$ lies on or poleward of $\theta_{stir}$. The propensity for the jet to lie poleward of the stirring latitude is due to the preferentially-equatorward propagation of the eddies, but at high stirring latitudes, we will argue that the jet can no longer be sustained at the latitude of stirring and so it is found equatorward of the stirring region.

Barnes et al. (2010) showed that as the mean jet is located nearer to the pole, the easterlies on the poleward flank vanish due to a lack of wave-breaking and associated deceleration of the winds there. Indeed, Fig. 3a shows a similar result. We follow Barnes et al. (2010) and diagnose eddy propagation and wave-breaking by defining a wavenumber $K^*$,

$$K^* = \left( \frac{q_y \cos^2 \theta}{u - c} \right)^{1/2}, \tag{4}$$

where $q_y$ is the meridional gradient of absolute vorticity and c is the phase speed of the

wave. According to linear theory, zonal wavenumber $k$ turns when it reaches the latitude where $K^* = k$ and propagates toward larger values of $K^*$, breaking near its critical latitude, found where $K^*$ is large (Hoskins and Karoly 1981; Held 1983). $K^*$ is plotted in Fig. 3c and shows that when $\theta_{stir} = 35^o$, the eddies break on both flanks of the jet, producing easterlies. However, when $\theta_{stir} = 65^o$ only one critical latitude appears on the equatorward flank, and thus there are no easterlies on the poleward flank of the jet.

The question remains, how does the variability of the jet change as $\theta_{edj}$ is located closer to the pole? Histograms of jet latitude $Z_{lat}$ are plotted in Fig. 3c and show that jets closer to the pole move around less than those closer to the equator. To explore this change in jet variability with latitude, we define two more time series to describe the variability of the jet. $Z_{speed}$ is the daily maximum zonal-mean zonal wind strength and captures the daily strengthening and weakening of the jet peak. In addition, we utilize Empirical Orthogonal Function (EOF) analysis to define the mode of variability that describes the largest variance of the zonal-mean zonal wind field, and denote the associated principal component time series as $Z_{eof1}$.

Fig. 4b displays the percent of the total variance of the zonal-mean zonal wind field explained by each of the three time series ($Z_{lat}, Z_{speed}, Z_{eof1}$). The histograms in Fig. 3b suggest that the jet shifts less at higher latitudes, and indeed, Fig. 4b shows that $Z_{lat}$ explains less of the total variance at high latitudes. In contrast, $Z_{speed}$ explains more of the variance at high latitudes. The leading EOF captures the pattern that accounts for the highest percentage of the total variance, and we see that at low to mid latitudes, $Z_{eof1}$ appears similar to $Z_{lat}$, but at latitudes above 55°N, the leading mode of variability is described by the speed of the jet, not its shift. This is seen in Fig. 4c where we plot the magnitude of

the jet shift, defined as the meridional distance between the latitude of the mean jet and the latitude of the jet associated with 1 standard deviation of $Z_{eof1}$. As the jet moves poleward, the leading mode of variability is associated less with meridional movement and more with the strength of the jet.

We can understand these changes in variability with latitude by considering the influence of the pole on eddy propagation and wave-breaking. The strength of the positive feedback between the zonal-flow and the eddies depends upon the ability of the mean-flow to influence the eddies by setting the critical latitudes, and in turn, the ability of the eddies to influence the jet by decelerating the flow where they break and fluxing momentum back into the jet core. When the jet is far from the pole, random fluctuations of the eddy forcing shift the jet, which shifts the critical latitudes, which in the end, shifts the distribution of momentum flux such that the jet can be maintained in its new position.

When the jet is near the pole, random fluctuations of the eddy forcing may still move the eddy-driven jet poleward, but the small value of $\cos^2\theta$ and $\beta$ in (4) will inhibit the jet from defining a new poleward critical latitude. Since the critical latitudes set the eddy-momentum flux distribution, the eddy-driven jet will not be sustained there. Profiles of $K^*$ suggest that only the largest waves can propagate near the pole, and this result is consistent with the shift of the eddy-length scale to larger wavelengths as the stirring moves poleward, as seen in Section 3.

In the real atmosphere, the dominant variability of the midlatitude jet involves both a shift and a pulse. The leading mode of variability of the North Atlantic jet is termed the North Atlantic Oscillation (NAO) and describes oscillations between an equatorward eddy-driven jet and a poleward, strengthened jet (Hurrell et al. 2003). Woollings et al.

(2010) argue that characterizing the full-range of variability of the North Atlantic jet requires descriptions of both the strength and the latitudinal position of the jet. Both of these results are consistent with our findings that the variability of a jet in midlatitudes experiences a mix of shifting and pulsing variability due to its proximity to the pole.

Section Summary

As the eddy-driven jet moves poleward:

- the leading mode of variability of the eddy-driven jet changes from a meridional shift to a pulse of the jet.
- the feedback between the zonal-flow and the eddies is reduced due to the inability of the eddies to propagate and break at high latitudes.

# 5. Dynamics of a pulsing jet

Previous studies have demonstrated that a pulse of the eddy-driven jet is less persistent than a meridional shift of the jet due to the presence of a positive eddy feedback during the shifting mode and no such feedback during a pulsing mode (Lorenz and Hartmann 2001; Eichelberger and Hartmann 2007). Here, we suggest a mechanism for the presence of a negative feedback during pulsing mode events, which forces the jet back to its equilibrium state and accounts for the lack of persistence.

Fig. 5a shows composites of the zonal wind of the $\theta_{stir} = 35^{o}$N integration for the top and bottom 10% of $Z_{speed}$. From these profiles, it is clear that when the jet strengthens, $u$

becomes large and $q_y$ increases in (4). The profiles of $K^*$ associated with these wind fields are plotted in Fig. 5b for $c = 1 - 4$ m/s and show that ultimately, $K^*$ decreases at the jet core for strong winds, implying that only the largest Rossby waves can propagate within the stronger zonal flow. Profiles of $K^*$ for larger phase speeds results in similar profiles, although the critical lines move toward the jet center since $\overline{u} - c$ decreases. In Fig. 5b, the reduction of $K^*$ suggests that fewer waves are able to propagate and break away from the jet, and thus there is less momentum flux converging in the jet core two days after a strengthening event (Fig. 5c). This reduction in momentum flux convergence acts as a negative feedback on the stronger jet, and the jet subsequently weakens back to its original strength. A similar story is seen when the jet weakens from its equilibrium value. In this case, $K^*$ suggests that more waves are able to propagate away and break, and thus more momentum converges into the jet region. Once again, this is a negative feedback on a weakened jet, and the jet profile returns to its equilibrium value.

The linear diagnostic $K^*$ suggests that after a strengthening of the jet, the anomalous eddy-momentum flux across the jet flanks are *out of the jet*, acting to weaken the jet. Likewise, after the weakening of the jet, the anomalous eddy-momentum flux across the jet flanks are *into the jet*. To confirm that this is the case, we calculate lagged-correlations of $Z_{speed}$ and the anomalous eddy-momentum flux across latitude circles $10^o$ equatorward and poleward of the mean jet. The results for the $\theta_{stir} = 35^o$ integration are plotted in Fig. 6, where positive correlations imply eddy *propagation away from the jet* and positive lags imply that the jet leads the forcing. Focusing on the equatorward latitude circle first, there is a positive flux of momentum into the jet a day or two before a pulsing event, which is clear evidence of the eddies forcing the jet to strengthen. Lorenz and Hartmann (2001) showed that a positive

eddy-mean flow feedback manifests itself as positive correlations at positive lags, however, Fig. 6 shows that the net effect of the eddies is to extract momentum from the jet, returning the jet to its mean state.

Focusing on the poleward latitude circle of Fig. 6, one might be surprised to see that it is not identical to that of the equatorward curve, but rather, the momentum flux across this poleward latitude circle is *out of* the jet core at positive and negative lags. The reason for this is due to the linear Rossby wave propagation arguments of the previous sections, whereby the pole inhibits Rossby wave propagation. The eddies on the poleward flank do not propagate poleward as one might expect, but rather propagate equatorward as well, fluxing momentum poleward. Fig. 6 demonstrates that there is even more equatorward wave propagation on the poleward flank during a strengthening event, implying that even fewer waves are able to propagate poleward. This conclusion was also drawn from Fig. 5b, where $K^*$ suggests that fewer waves are able to propagate toward the pole when the jet strengthens and $q_y$ increases.

As the jet shifts poleward, the dominant variability changes from a shift to a pulse, and the eddies act as a negative feedback on the strengthening and weakening jet. Consistent with this mechanism, recent work has shown that the leading mode of variability becomes less persistent as the jet is found at higher latitudes, both in a barotropic model and in general circulation models (Barnes et al. 2010; Barnes and Hartmann 2010).

It is possible that barotropic instability on the poleward jet flank may also bring about the decay of a pulsing jet. However, for the wind profiles simulated by this model, only lowest zonal wavenumbers are unstable and the growth rates are very slow with e-folding times of weeks. In addition, eddy momentum fluxes by the unforced wavenumbers 1-3 contribute

little to the total momentum flux into and out of the jet during pulsing events (not shown), implying that normal mode growth on the polar flank of the jet cannot explain the decay of the pulsing mode in the model.

Section Summary

- When the jet strenghtens, $\overline{u}$ and $q_y$ increase, resulting in a modified $K^*$ profile.
- Plots of $K^*$ suggest that the eddies are less likely to propagate away from the jet core during a strengthening event, which acts as a negative feedback on the pulsing jet.
- For jets close to the pole, the eddies on the poleward flank are unable to propagate poleward, and thus the momentum flux is always away from the jet center. In this situation, the eddies on the equatorward side dominate the driving, and it is the convergence of poleward momentum flux that drives the pulsing of the jet.

# 6. Influence of the subtropical jet on eddy-driven jet variability

Thus far, we have looked poleward to determine the contraints on jet variability and the eddy-mean flow interaction set by the presence of $\beta$. In this section, we look equatorward to study the influence of a strong subtropical jet on the variability of the eddy-driven jet. We will demonstrate that the mechanisms which explain the dependence of eddy-driven jet variability on $\beta$ can also explain the influence of a subtropical jet on eddy-driving of the

midlatitude jet. More specifically, the subtropical winds can influence the location of the critical latitudes through modification of $u$ in (4), thus breaking the positive feedback loop between the eddies and the eddy-driven jet and subsequently changing the variability of the eddy-driven jet.

To analyze the influence of the subtropical jet on eddy-mean flow interactions, the latitude of the subtropical jet ($\theta_{sub}$), is varied every 5° between 20°N and 45°N and the eddy stirring is fixed at $\theta_{stir} = 45$°N for all integrations, with stirring over total wavenumbers $8 \leq l \leq 12$ and $m \geq 4$. While moving the eddy-driven jet and fixing the latitude of the subtropical jet may be more physically related to understanding seasonal and regional variability, we present results for a fixed eddy stirring latitude to remove the effect of latitude on eddy wave propagation discussed previously.

The subtropical jet is modeled as a Gaussian in zonal wind

$$u_{sub}(\theta) = \mathcal{U} \exp\left(\frac{-(\theta - \theta_{sub})^2}{2\sigma_{sub}^2}\right), \tag{5}$$

where $\sigma_{sub} = 6$° and $\mathcal{U}$ is the speed of the subtropical jet, which is set to 20 m/s. The vorticity equation from (1) is integrated forward with the stirring ($\mathcal{S}$) and relaxed back to the subtropical jet profile $\zeta_{sub}$ derived from (5)

$$\frac{\partial \zeta}{\partial t} + u\frac{\partial \zeta}{\partial x} + v\frac{\partial \zeta}{\partial y} + v\beta = \mathcal{S} - r(\zeta - \zeta_{sub}) - \kappa\nabla^4(\zeta - \zeta_{sub}), \tag{6}$$

where values for $r$ and $\kappa$ are the same as in Section 4.

*a. Effect of subtropical winds on the latitude of the eddy-driven jet*

Fig. 7 displays diagnostics for three placements of the subtropical jet, with the zonal-mean zonal wind profiles plotted in Fig. 7a–c. The solid curve denotes the total zonal-mean zonal-wind, while the dashed line denotes the part associated with the fixed subtropical jet (5). Because the subtropical jet is held fixed throughout the integration, we subtract its profile from the total zonal-wind profile to obtain the "eddy-driven jet", or the part of the zonal wind that is driven by the eddies. When $\theta_{sub} = 20^{o}$, the total zonal-wind profile distinctly shows two separated jets. As $\theta_{sub}$ moves poleward, the subtropical and eddy-driven jets merge and become one strong jet, similar to that seen in the North Pacific and South Pacific during their respective winter seasons (Eichelberger and Hartmann 2007; Nakamura and Shimpo 2004).

A closer look at Fig. 7a–c shows that although the eddy stirring is centered at 45$^{o}$N in all integrations, the latitude of the maximum winds of the eddy-driven jet ($\theta_{edj}$) moves poleward with $\theta_{sub}$. Fig. 8a shows that this is true for all subtropical jet locations. Interestingly, Lee and Kim (2003) used an idealized model to demonstrate that the most favorable region for baroclinic wave growth and latitude of the eddy-driven jet is approximately 20$^{o}$-30$^{o}$poleward of a modest subtropical jet, in which case the eddy-driven jet is well separated from the subtropical jet. We will demonstrate that in a barotropic model, the separation between the eddy-driven and subtropical jets is due to the latitudes of eddy wave-breaking set by the background flow.

Since the critical latitudes depend on the difference between the eddy phase speeds and the background flow $u$, the presence of a subtropical jet has the potential to greatly influence

the location of eddy wave-breaking, and thus the location of the eddy-driven jet. Profiles of $K^*$ for the three integrations are plotted in Fig. 7d–f. When $\theta_{sub} = 20^o$, the subtropical winds act to widen the $K^*$ profile such that waves with $c = 1 - 4$ m/s are able to propagate farther equatorward before breaking. This manifests itself as a wider eddy-driven jet located close to the equator. As $\theta_{sub}$ moves poleward, the total zonal-wind profile becomes stronger and sharper, influencing both $u$ and $q_y$ in (4) and causing the equatorward critical latitude to move with the subtropical jet. This in turn acts to sustain the eddy-driven jet farther poleward than in the $\theta_{sub} = 20^o$ case.

*b. Effect of subtropical winds on the variability of the eddy-driven jet*

Eichelberger and Hartmann (2007) showed that the leading mode of the eddy-driven jet changes from a shift to a pulse in the presence of a strong subtropical jet due to the interaction of the subtropical winds with the baroclinic eddies. They suggest that the subtropical jet acts as a waveguide, allowing the eddies to propagate downstream, inhibiting the positive feedback between the eddies and the background flow. Our work suggests that similar relationships are found in the barotropic simulations, and we explore the reason for this interaction in this section.

Fig. 7g–i shows histograms of $Z_{lat}$ for different locations of the subtropical jet. As the subtropical jet moves poleward from 20°N to 40°N, the meridional movement of the eddy-driven jet is greatly restricted, indicated by the narrowness of the histogram. As done in Section 4, we calculate the daily time series of eddy-driven jet speed $Z_{speed}$ and the leading principal component $Z_{eof1}$ of the zonal-mean zonal wind to provide additional descriptions

of midlatitude jet variability. Fig. 8b displays the percent of the total variance of the zonal-mean zonal wind field explained by each of the three time series ($Z_{lat}, Z_{speed}, Z_{eof1}$). As the subtropical jet moves toward the eddy stirring latitude, the variability of the eddy-driven jet changes from a shifting to a pulsing, reminiscent of the jet behavior near the pole in Fig. 4b. To confirm that the leading mode of variability is changing from a shift to a pulse of the jet (although it describes similar percentages of the variance across all integrations), Fig. 8c displays the shift of the eddy-driven jet associated with 1 standard deviation of $Z_{eof1}$. As the subtropical jet is moved toward the latitude of stirring (45°N), the magnitude of the shift of the eddy-driven jet decreases until the leading mode no longer describes a shift of the jet.

These results are easily understood by applying the same reasoning as in Section 4. When a subtropical jet is present, the critical latitudes are set by the location of the strong subtropical winds. Thus, the positive feedback chain between the eddies and the eddy-driven jet is broken: the eddies continually break and reinforce the eddy-driven jet, but the eddy-driven jet does not set the latitude of breaking since the winds are too weak and are dominated by the strong subtropical winds. Thus, the distribution of momentum flux convergence is set by the stationary subtropical jet, inhibiting movement of the eddy-driven jet. In this case, the eddy-driven jet cannot move meridionally, but can strengthen and weaken since this does not require movement of the critical latitudes.

### Section Summary

As the subtropical jet moves poleward toward the latitude of the eddy-driven jet:

- the eddy-driven jet also shifts poleward due to the influence of the strong subtropical

winds on the eddy wave-breaking latitudes.

- the leading mode of variability of the eddy-driven jet changes from a meridional shift to a pulse of the jet.

# 7. Discussion & Conclusions

Eddy-driven jet variability is influenced by the location of critical latitudes and eddy wavebreaking. On the equatorward side of the jet, the presence of a strong subtropical jet causes the eddy-driven jet variability to change from a shift to a pulse due to a reduction in the positive feedback between the eddies and the mean flow by the strong subtropical winds. On the poleward side of the eddy-driven jet, the effects of $\beta$ on Rossby wave propagation produces similar changes in the eddy-mean flow interaction, causing the leading mode of variability to change from a shift to a pulse of the jet.

This work identifies a robust increase in eddy-length scale as the jet is located at higher latitudes in a non-linear barotropic model, which highlights that the latitude of the eddy-driven jet and the characteristic eddy scale are inextricably linked. We find that the eddy length scales proportionally to the Rhines scale, which predicts an increase in eddy-length scale of about 5% for a jet moving from 46° to 48.5°, and which agrees with what is seen in global warming simulations (Kidston et al. 2010).

While this work analyzed an idealized barotropic model, the question "how might the pattern of atmospheric variability change with a poleward shift of the jet?" is applicable to the real atmosphere. This work suggests that the "annular modes" will transition from a

shift to a pulse of the zonal-mean zonal winds as the eddy-driven jet moves poleward with climate change. In addtion, results presented here suggest that the expansion of the Hadley cell alone has the potential to shift the eddy-driven jets poleward, even in the absence of a change in midlatitude dynamics. Additional analysis of more complex models is required to determine whether these mechanisms are dominant in the real atmosphere.

*Acknowledgments.*

This work supported by the Climate Dynamics Program of the National Science Foundation under grant ATM 0409075.

# REFERENCES


Barnes, E. A. and D. L. Hartmann, 2010: Testing a theory for the effect of latitude on the persistence of eddy driven jets using the CMIP3 simulations. *Geophys. Res. Lett.*, **37**, L15 801, doi:10.1029/2010GL044144.

Barnes, E. A., D. L. Hartmann, D. M. W. Frierson, and J. Kidston, 2010: The effect of latitude on the persistence of eddy-driven jets. *Geophys. Res. Lett.*, **37**, L11 804, doi: 10.1029/2010GL043199.

Eichelberger, S. J. and D. L. Hartmann, 2007: Zonal jet structure and the leading mode of variability. *J. Climate*, **20**, 5149–5163, doi:10.1175/JCLI4279.1.

Held, I. M., 1983: Stationary and quasi-stationary eddies in the extratropical troposphere: Theory. *Large-scale dynamical processes in the atmosphere*, B. J. Hoskins and R. P. Pearce, Eds., Academic Press, London, 127–168.

Hoskins, B. J. and D. J. Karoly, 1981: The steady linear response of a spherical atmosphere to thermal and orographic forcing. *J. Atmos. Sci.*, **38**, 1179–1196.

Hurrell, J. W., Y. Kushnir, G. Ottersen, and M. Visbeck, 2003: An overview of the North Atlantic Oscillation. *The North Atlantic Oscillation: Climatic Significance and Environmental Impact*, Amer. Geophys. Union, No. 134 in Geophysical Monotraph.

Kidston, J., S. M. Dean, J. A. Renwick, and G. K. Vallis, 2010: A robust increase in

the eddy length scale in the simulation of future climates. *Geophys. Res. Lett.*, **37**, doi: 10.1029/2009GL041615.

Kidston, J. and E. Gerber, 2010: Intermodel variability of the poleward shift of the austral jet stream in the CMIP3 integrations linked to biases in the 20th centery climatology. *Geophys. Res. Lett.*, **37**, L09 708, doi:10.1029/2010GL042873.

Lee, S. and H.-K. Kim, 2003: The dynamical relationship between subtropical and eddy-driven jets. *J. Atmos. Sci.*, **60**, 1490–1503.

Lorenz, D. J. and D. L. Hartmann, 2001: Eddy-zonal flow feedback in the Southern Hemisphere. *J. Atmos. Sci.*, **58**, 3312–3327.

Nakamura, H. and A. Shimpo, 2004: Seasonal variations in the Southern Hemisphere storm tracks and jet streams as revealed in a reanalysis dataset. *J. Climate*, **17**, 1828–1844.

Rhines, P. B., 1975: Waves and turbulence on a beta-plane. *J. Fluid Mech.*, **69**, 417–443.

Smith, K., G. Boccaletti, C. Henning, I. Marinov, C. Tam, I. Held, and G. Vallis, 2002: Turbulent diffusion in the geostrophic inverse cascade. *J. Fluid Mech.*, **469**, 13–48.

Vallis, G. K., E. P. Gerber, P. J. Kushner, and B. A. Cash, 2004: A mechanism and simple dynamical model of the North Atlantic Oscillation and annular modes. *J. Atmos. Sci.*, **61**, 264–280.

Woollings, T., A. Hannachi, and B. Hoskins, 2010: Variability of the North Atlantic eddy-driven jet stream. *Quart. J. Roy. Meteor. Soc.*, **136**, 856–868, doi:10.1002/qj.625.

# List of Tables

Table 1: definitions

| | |
|---|---|
| $\theta_{sub}$ | latitude of the center of the subtropical jet |
| $\theta_{edj}$ | latitude of the resulting eddy-driven jet |
| $\theta_{stir}$ | latitude of the center of the stirring |
| $Z_{lat}$ | daily time series of the latitude of the eddy-driven jet |
| $Z_{speed}$ | daily time series of the maximum speed of the eddy-driven jet |
| $Z_{eof1}$ | daily time series of the leading EOF of zonal-mean zonal wind |
| $\hat{l}$ | peak total wavenumber of the vorticity spectrum |
| $l_R$ | total wavenumber predicted by the Rhines scale |

# List of Figures

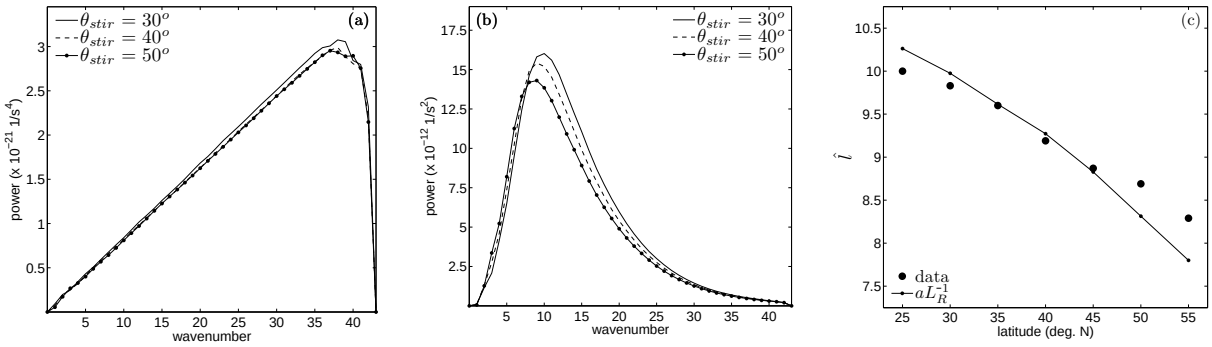


Figure 1: (a) Vorticity stirring ($\mathcal{S}$) power versus total wavenumber $l$ after windowing the field. (b) Vorticity power versus total wavenumber. (c) The wavenumber at which the eddy vorticity spectrum is maximum ($\hat{l}$) for all experiments. The wavenumbers predicted by the Rhines scale $l_R = aL_R^{-1}$ are also plotted (see text for details).

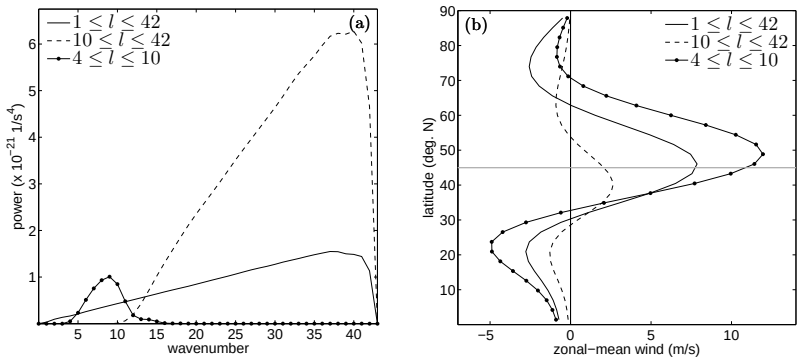


Figure 2: (a) Vorticity stirring ($\mathcal{S}$) power versus total wavenumber $l$ after windowing the field. (b) Zonal-mean zonal-wind profiles. In all three experiments, the zonal wavenumber $m$ was restricted to the same range as $l$.

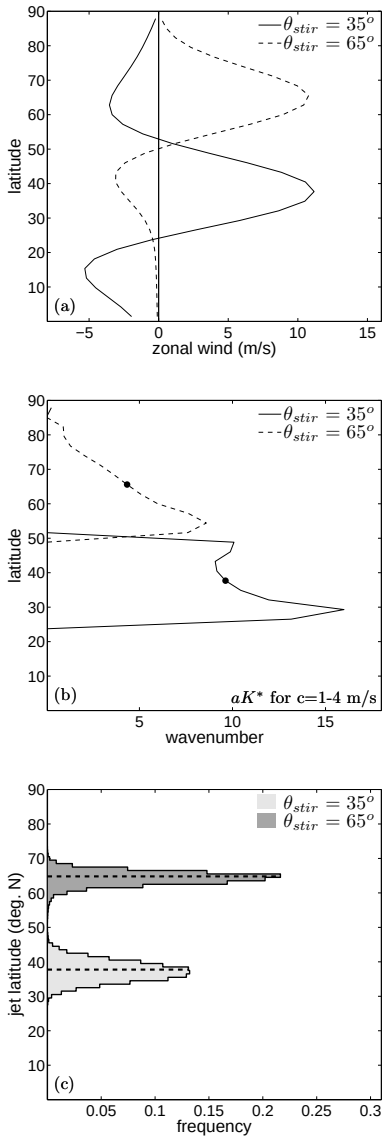


Figure 3: (a) Average zonal-mean zonal wind profiles for integrations where the stirring latitude is varied. (b) $K^*$ times the radius of the earth $a$ averaged for phase speeds of 1-4 m/s. The filled circle denotes the latitude of the eddy driven jet ($\theta_{edj}$) where the calculation was centered. (c) Histograms of daily eddy-driven jet latitude ($Z_{lat}$) frequency for different $\theta_{stir}$. Mean jet latitudes are plotted as thick dashed horizontal lines.

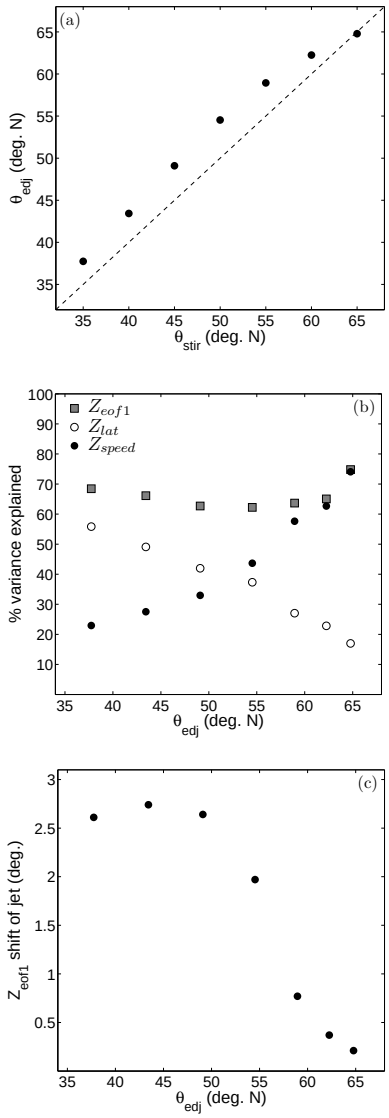


Figure 4: (a) The latitude of the eddy-driven jet ($\theta_{edj}$) versus the latitude of eddy stirring ($\theta_{stir}$). The dashed line denotes the one-to-one line. (b) The percent of the total variance of the zonal-mean zonal wind explained by $Z_{eof1}$, $Z_{lat}$ and $Z_{speed}$. (c) The shift of the eddy-driven jet associated with one standard deviation of the leading EOF ($Z_{eof1}$) versus $\theta_{edj}$ for integrations with varying stirring latitudes.

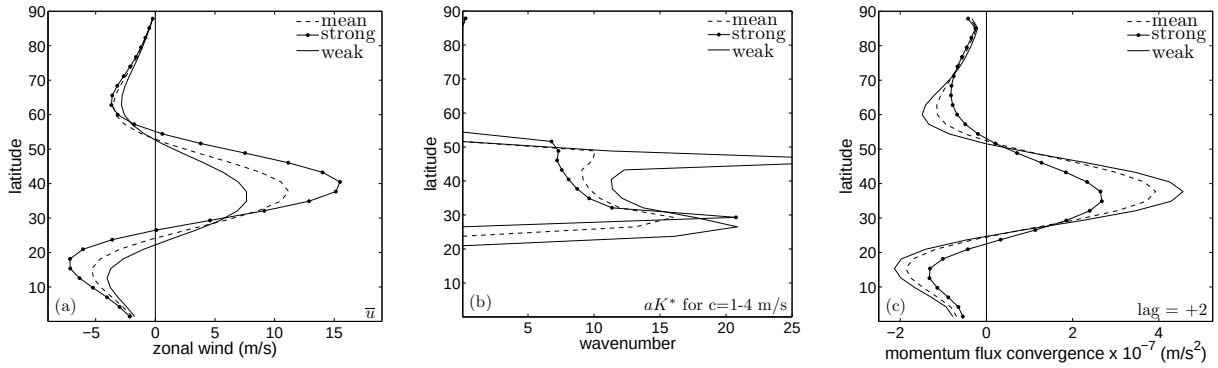


Figure 5: (a) Zonal-mean zonal wind profiles for the mean and extremely strong and weak jet strength days. (b) $K^*$ times the radius of the earth $a$ for the mean and extremely strong and weak jet strength days for phase speed $c = 1-4$ m/s. (c) Profiles of the eddy momentum-flux convergence for the mean and two days after extremely strong and weak jet strength days. Plots are of the $\theta_{stir} = 35^{\circ}$N integration.

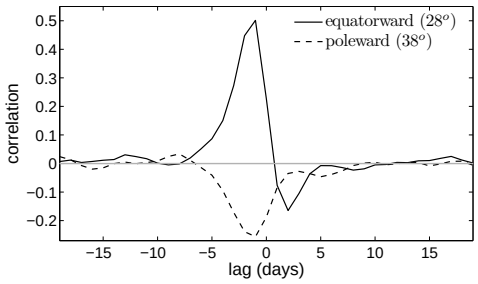


Figure 6: Lagged-correlation over all pulsing days of $Z_{speed}$ and the eddy propagation *away from* the jet core at latitudes 10° equatorward and poleward of the time-mean jet for $\theta_{stir} = 35°$.

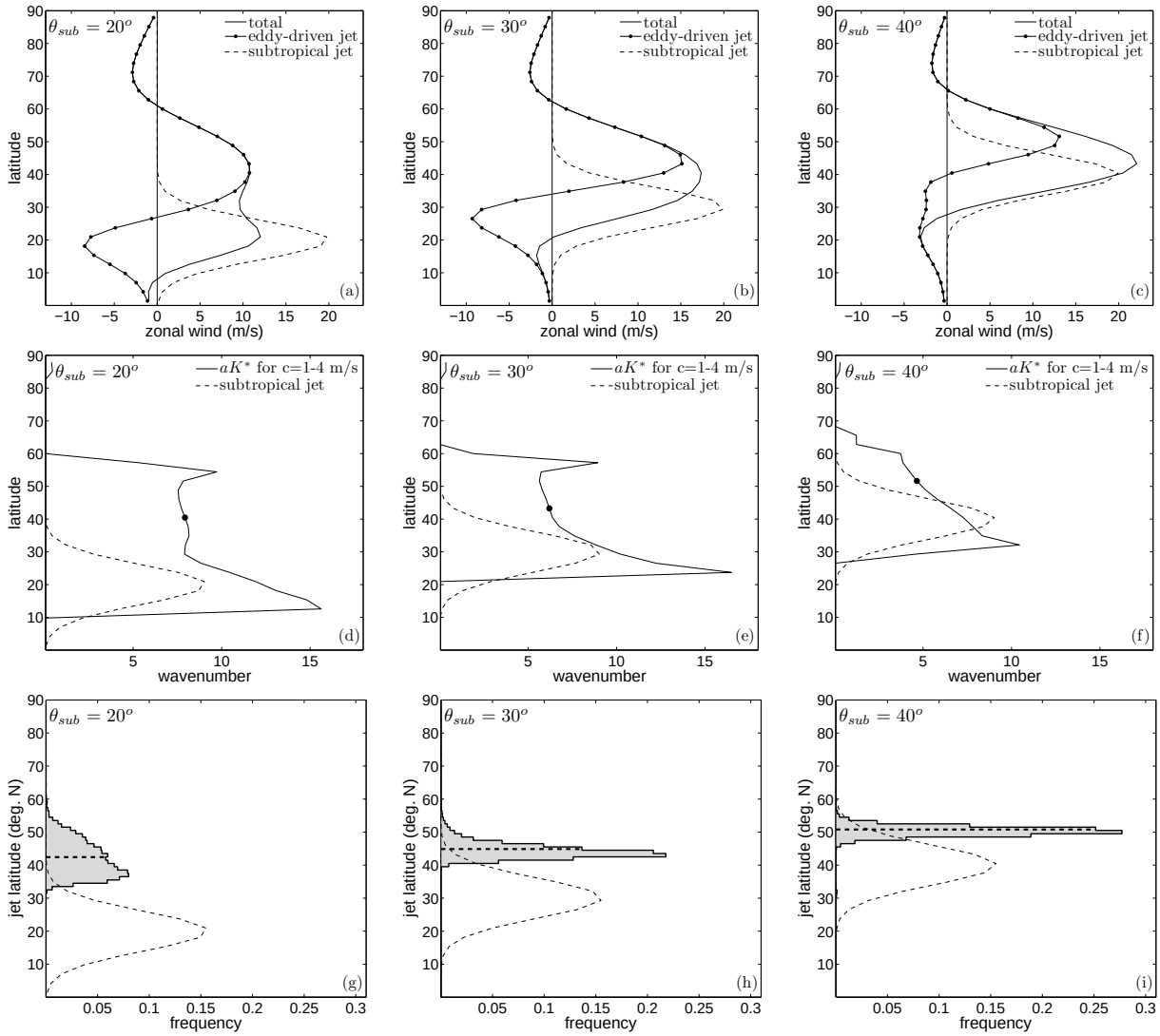


Figure 7: (a)–(c) Average zonal-mean zonal wind profiles for integrations where the subtropical jet latitude is varied. The eddy-driven jet profile is defined as the difference between the total wind profile and the subtropical jet. (d)–(f) $K^*$ times the radius of the earth $a$ averaged for phase speeds of 1-4 m/s. The filled circle denotes the latitude of the eddy driven jet ($\theta_{edj}$) where the calculation was centered. The subtropical jet profile is plotted in arbitrary units. (g)–(i) Histograms of daily eddy-driven jet latitude ($Z_{lat}$) frequency for different subtropical jet placements. Mean jet latitudes are plotted as thick dashed horizontal lines. The subtropical jet profile is plotted in arbitrary units.

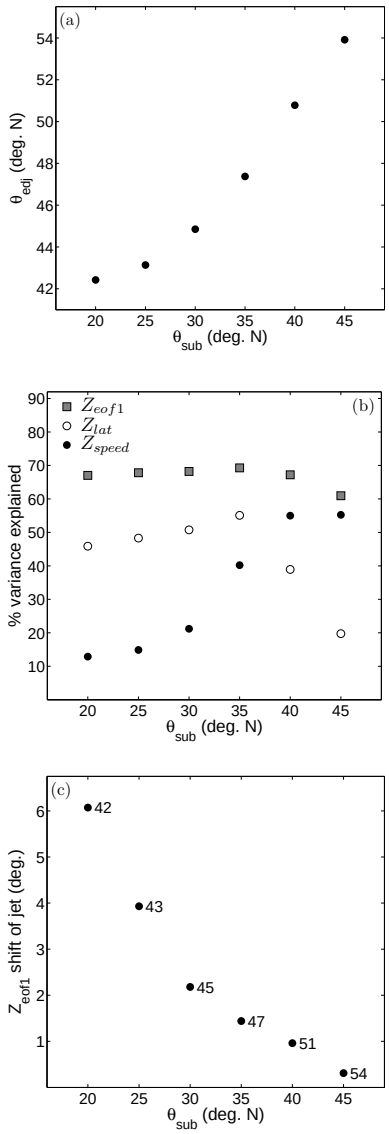


Figure 8: (a) The latitude of the eddy-driven jet ($\theta_{edj}$) versus the latitude of the subtropical jet ($\theta_{sub}$). (b) The percent of the total variance of the zonal-mean zonal wind explained by $Z_{eof1}$, $Z_{lat}$ and $Z_{speed}$. (c) The shift of the eddy-driven jet associated with one standard deviation of the leading EOF ($Z_{eof1}$) versus $\theta_{sub}$. $\theta_{edj}$ is denoted next to each marker for reference. The eddy stirring is at 45°N for all integrations.